Reprinted from The Journal of Physical Chemistry, 1992, 96.

Probing Double-Minima Ion–Molecule Reaction Coordinates by Photoelectron Spectroscopy of Clusters: $PhOH^+ + NH_3 \rightarrow PhO + NH_4^+$

Jack A. Syage* and Jhobe Steadman

The Aerospace Corporation, P.O. Box 92957/M5-754, Los Angeles, California 90009
(Received: September 17, 1992; In Final Form: October 6, 1992)

Recently, we reported the direct detection of two distinct and stable reactive complexes confirming a double-minima barrier process for the reaction $PhOH^+ + NH_3 \rightarrow PhO + NH_4^+$ (Steadman, J.; Syage, J. A. *J. Am. Chem. Soc.* **1991**, *113*, 6786). A model explaining the origin of the barrier and its generality to proton-transfer reactions involving delocalized charge was also presented. However, in that study, the barrier height could not be experimentally estimated because the ion–complex energy distribution was not known. In this report, we present photoelectron spectra to measure the energy distribution of the complex form $PhOH^+\cdots(NH_3)_n$ produced by resonance two-photon ionization of the corresponding neutral clusters. The collective photoelectron and mass spectra results indicate that the barrier to proton transfer from the reactive complex is 1.0–1.5 eV.

Introduction

Photoexcitation of van der Waals (vdW) complexes is a useful way to study the bound and quasibound reactive complexes associated with gas-phase bimolecular collisions.[1,2] Ionization of vdW complexes to form reactive complexes of ion–molecule reactions[3-8] is especially favorable because they tend to be stable due to charge-induced dipole interactions, in contrast to neutral–neutral complexes which are often unbound and associated with a saddle-point region on a potential energy surface. Our past experiments on reactivity of molecular complexes have given us a new understanding of gas-phase chemistry as well as core solvation effects relevant to condensed-phase chemistry.[7-11] In this paper, we report on the use of photoelectron spectroscopy of clusters to probe details of reactive complexes trapped in double-minima ion–molecule potentials.

Ion–molecule kineticists, for many years, have postulated that some reactions (mostly fast) proceed along barrierless single-well reaction coordinates whereas other reactions (mostly slow) involve double-well barrier processes.[12] Included in the latter group are classes of reactions in which the charge distribution in the reactant is delocalized from the eventual charged leaving group. The double-minima barrier mechanism[12,13] became widely accepted well before the existence of two distinct and stable reactive complexes was experimentally confirmed.[8] $PhOH^+$ is an acid cation that has a ground electronic-state charge distribution delocalized from the potential proton leaving group, which prompted us to investigate the possibility of detecting two stable complex forms with NH_3. Using a picosecond delayed-ionization technique, we confirmed the existence of a double-minima reaction coordinate for $PhOH^+ + NH_3 \rightarrow PhO + NH_4^+$ by establishing the stability of the two reactive complexes $PhOH^+\cdots(NH_3)_n$ and $PhO\cdots H^+(NH_3)_n$.[8] A model for the potential energy surface showed that the barrier is due to a surface crossing and should be a general feature for ion–molecule reactions in which the reactant charge is delocalized from the leaving group (Figure 1, cf. Discussion).

The surface-crossing barrier model predicts an upper limit to the barrier height of about 1.5 eV above the reactive complex minimum energy. However, the barrier height could not be determined in our previous experiment because the energy distribution of the reactive complex, produced by resonance two-photon ionization of the corresponding neutral cluster, was not known.[8-10] In this work we measure the energy distribution by photoelectron spectroscopy and compare the results to the yield of proton-transfer products $PhO + H^+(NH_3)_n$ in order to estimate barrier heights. This work also provides the opportunity to introduce a new design in molecular beam photoelectron spectroscopy.

Experimental Section

These experiments make use of a new time-of-flight (TOF) photoelectron spectrometer equipped with a paraboloidal electrostatic reflector (PER), shown in Figure 2, to enhance electron collection efficiency.[14,15] The PER improves the effective solid angle of detection by 1–2 orders of magnitude compared to conventional TOF spectrometers that collect only detector line-of-sight electrons. Two paraboloidal grid forms, separated by 1 mm at the apex, are biased to create a reflecting field for electrons (−5 V in this study). A skimmed molecular beam enters the PER through a hole in the apex and is crossed by a laser that enters and exits through two holes in the side. The intersection takes place at the focal point of the PER. All reflected electrons become collimated and travel the same path length of 1 m toward the detector. A 20-fold enhancement is observed for reflected electrons versus direct electrons. The direct electrons are currently unblocked and arrive at the detector about 2% sooner than reflected electrons of the same energy. The inner paraboloid and flat grid are maintained at ground potential. A 1-V acceleration potential across the flat grid region was used to enhance detection efficiency, particularly at low energy.

The paraboloid outer circumference matches the drift tube diameter of 9 cm. We employ a 4-cm-diameter detector, which necessitates the use of an einsel lens assembly at the drift tube end to focus the electrons onto the detector. The PER and drift tube are shielded from stray magnetic fields by two layers of μ-metal. The signal levels are sufficiently high to permit the use of analog current measurements using a fast digital storage oscilloscope (350- and 400-MHz sampling rate) and built-in signal averaging. The intensity resolution of the digitized spectra is compromised somewhat in the present case of broad photoelectron spectra because of a dilution of electron counts per time channel. The averaged intensities are considerably less than the full vertical scale necessary to detect single-electron pulses. A few bits of vertical resolution are consequently lost, causing a binning effect on the digitized intensities. The analog spectra, which do not suffer from this effect, are saved to verify that they are reliably reproduced by the digitized spectra. Although the cluster photoelectron spectra in Figure 3 are inherently broad, the resolving power of the instrument can achieve the larger of $\Delta E = 10$ meV or $\Delta E/E = 0.01$. Twice these values, though, would be typical operating conditions. A complete description of the apparatus will be published elsewhere.[14]

A phenol sample was placed in a temperature-controlled pulse valve maintained at about 40 °C. A mixture of 2% NH_3 in Ar was flowed into the pulsed valve at 30 psia pressure. The laser and pulsed valve were operated at 10 Hz. Nanosecond and picosecond resonance two-photon ionizations were used to record the photoelectron spectra. Nanosecond excitation wavelengths were tuned near the origins of the $PhOH\cdot(NH_3)_n$ clusters.[16] The $S_1 \leftarrow S_0$ spectra for clusters $n > 2$ are broad, making it difficult to ionize specific cluster sizes;[16] however, because the origin transitions undergo red shifts with increasing n, it is possible to vary the low cluster size cutoff. The falloff in the cluster dis-

0022-3654/92/2096-9606$03.00/0

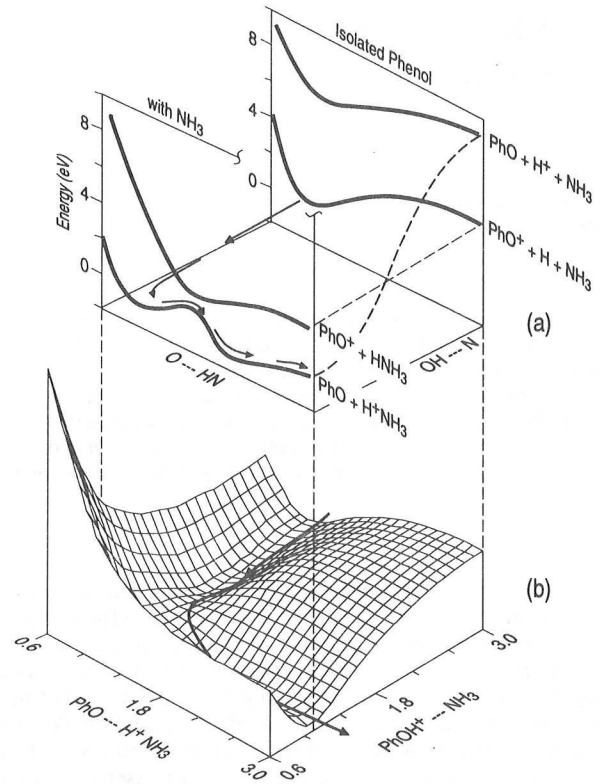

Figure 1. Model of the potential energy reaction coordinate for the reaction $PhOH^+ + NH_3 \rightarrow PhO + NH_4^+$. (a) Potential energy curves for uncomplexed and complexed $PhOH^+$ showing the surface crossing that gives rise to the barrier to proton transfer. (b) A rendition of the lower adiabatic potential energy surface for the collinear O···H···N coordinate (in Å). Reaction paths are drawn for visualization in (a) and (b).

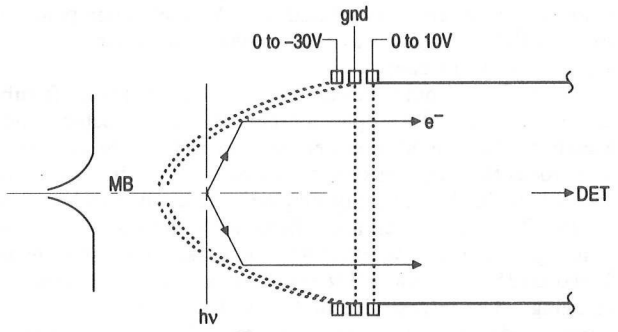

Figure 2. Schematic of the paraboloidal electrostatic reflector (PER) used for the TOF photoelectron spectrometer. A collimated molecular beam is crossed with the laser at the paraboloid focal point, and the photoelectrons are reflected and collimated in the direction of the detector. These experiments used a reflecting potential of −5 V and an acceleration potential into the drift tube of 1 V.

tribution to higher n was adjusted by varying the NH_3 fraction in the expansion (e.g., a lean mixture causes a faster falloff). Picosecond excitation at 266 nm is well above the origins of all clusters so these results sampled a large cluster distribution. The conditions for controlling cluster ion distributions were determined using mass spectrometry.[8,9]

Results

Photoelectron spectra of $PhOH\cdot(NH_3)_n$ clusters are plotted in Figure 3 for various excitation wavelengths, pulse duration, and expansion conditions. The electron energy distribution is given by the difference in the photon energy and the ion energy distribution. The high-energy limits for electrons based on measured cluster ionization potentials[16] are indicated in Figure 3. The photoelectron spectra are broad for several reasons; for example, (1) rapid intramolecular vibrational redistribution (IVR) in the S_1 state gives rise to ionization transitions from a broad distribution

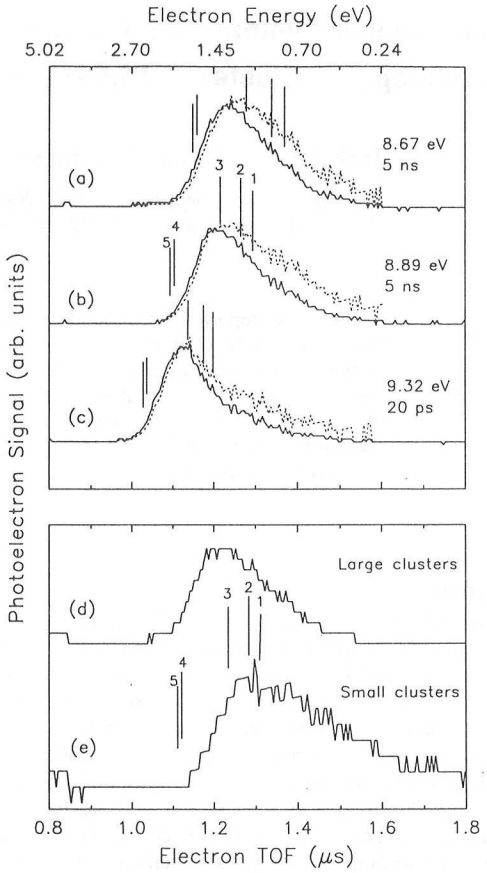

Figure 3. Photoelectron spectra for resonance two-photon ionization of $PhOH\cdot(NH_3)_n$ clusters: (a) 286-nm excitation, $n_{max} \sim 4$–5; (b) 279-nm excitation, $n_{max} \sim 3$; (c) 266-nm excitation, $n_{max} \sim 3$–4; (d) 280-nm excitation at the center of gas pulse, $n_{max} \sim 4$; (e) 280-nm excitation at edge of gas pulse, $n_{max} \sim 2$. The n_{max} values are estimated from mass spectra and knowledge of cluster $S_0 \leftarrow S_1$ transition energies. The vertical lines represent IPs for clusters of size n. The dotted curves in (a)–(c) are corrected for electron kinetic energy detection efficiency. The intensity resolution of spectra d and e is explained in the Experimental Section.

of bath states, (2) there exist low-frequency intermolecular modes that are Franck–Condon active for ionization, and (3) electron spectra overlap for different cluster sizes. Despite the broad and overlapping spectra, it is evident that the cluster ions are formed with substantial energy for all values of n.

The photoelectron spectrum for cluster sizes $n > 4$ is given in Figure 3a and is achieved by using an excitation wavelength of 286 nm that is to the red of the $S_1 \leftarrow S_0$ origin transition for the smaller cluster sizes.[16] The ionization potentials (IP) for $n = 4$ and 5 are both reported to be 6.89 eV (vs 8.51 eV for isolated phenol),[16] corresponding to maximum electron energies of 1.78 eV. There is clearly a large contribution in Figure 3a from ions with greater than 1 eV of ion energy. The photoelectron spectrum for 279-nm excitation is given in Figure 3b. Though excitation is to higher energy of the origin of all cluster sizes,[3,16] 279 nm is only resonant with the unstructured spectra for $n > 2$. (The mass spectrum peaks at $n = 3$.) The photoelectron energies for zero-energy ions of $n = 3$ and 4 are 1.38 and 2.0 eV, respectively. Again, the ion energy distribution extends to relatively high energy.

The photoelectron spectra in Figure 3 are due to ionization of complex form $PhOH^+\cdots(NH_3)_n$ and not $PhO\cdots H^+(NH_3)_n$. The latter complex is produced if the intermediate S_1 state undergoes excited-state proton transfer (ESPT) before ionization. This occurs in about 60 ps for $n \geq 5$ at 2500 cm^{-1} above the S_1 origin.[9] To avoid the possibility of ESPT, we recorded the spectrum in Figure 3c using prompt (20-ps, 266-nm) excitation/ionization. The photoelectron energies for the ion origins of $n = 3$ and 4 are 1.81 and 2.43 eV, respectively. The ion energy distribution is similar to the cases using longer wavelength nanosecond excitation. The

spectra in Figure 3d,e demonstrate that the cluster ions for n = 1 and 2 are also formed with substantial energy. These spectra compare the results for a large cluster distribution (not greatly exceeding $n = 6$) produced by ionization in the cold central portion of the gas pulse (Figure 3d) and for a small cluster distribution (dominated by $n \leq 3$) produced by ionization resonant with n = 1 in the warm leading edge of the gas pulse (Figure 3e). The latter spectrum shows that the energy distribution in these cluster ions extends to high energy.

We estimate that the fraction of cluster ions with greater than 1 eV of energy is at least 10% for all values of n considered here. The spectra in Figure 3 (solid lines) are not corrected for the electron energy detection efficiency $\eta(E)$, which has approximately the dependence $\eta = E^{-p}$. Under current operating conditions, p lies roughly between one and two. To obtain a better indication of the actual ion energy distributions, we have plotted alongside Figure 3a–c (dotted lines) spectra corrected for η using a value of $p = 1$.

Discussion

To understand the present experiment, it is necessary to review some of the results of our earlier work.[8,9] The model proposed for the potential energy surface and reaction coordinate is pictured in Figure 1.[8] Potential energy curves along the O–H coordinate are drawn for isolated $[PhOH]^+$ (back panel) and for $[PhOH\cdot NH_3]^+$ (front panel). The N–H coordinate running from back to front represents the approach of reactants in a bimolecular reaction, and the O–H coordinate, just mentioned, represents departure of products. The reaction coordinate is approximated by the path marked by arrows. The barrier is predicted on the basis of a simple concept. The ground electronic state of $PhOH^+$ dissociates to $PhO^+ + H$. The dissociative limit for $PhO + H^+$ is about 5 eV higher in energy (given by the difference in the ionization potentials of PhO and H, 8.56 and 13.60 eV, respectively)[17] and is probably associated with some higher unknown excited electronic state of $PhOH^+$. This dissociative limit is stabilized enormously as NH_3 approaches along the N–H coordinate because of the substantial 8.86-eV proton affinity[18] of NH_3. Because the ground-state dissociative limit $PhO^+ + H$ experiences considerably less stabilization from NH_3, the dissociative limits are reversed in energy by the approach of reactant NH_3 (dotted lines, Figure 1a). This causes a surface crossing that creates the barrier to reaction. The surface crossing reaction barrier should be a general property of reactions in which the charged leaving group is not the lowest energy dissociative limit of the isolated ion. And this situation will be typical of ions where charge is delocalized from the leaving group. A visualization of the shape of the lower adiabatic surface for the collinear O···H···N coordinate, based on the model in ref 8, is given in Figure 1b. The reaction path drawn represents the lowest energy reaction coordinate in the classical limit (ignoring zero-point energy).

Prior evidence that the barrier to proton transfer of $PhOH^+\cdots NH_3$ is large was reported by Mikami and co-workers[3] and by our laboratory.[8] The former experiment used nanosecond two-color resonance threshold ionization to measure the ionization potential of the complex $PhOH\cdot NH_3$ (7.71 eV) and the appearance potential for producing $PhOH^+ + NH_3$ (8.72 eV).[3] No NH_4^+ was observed, implying that proton transfer either is impeded by a large barrier or forms a very stable product complex $PhO\cdots H^+NH_3$ that does not readily dissociate. Our picosecond ionization work permitted selective formation of either the reactant or product ion complex by timing the ionization from the reactant and product of the excited-state reaction

$$PhOH^*\cdots(NH_3)_n \rightarrow PhO^{*-}\cdots H^+(NH_3)_n$$

which occurs only for $n > 4$ in about 60 ps.[8] For excess photoionization energy ranging from 1.2 to 2.4 eV, the $PhOH^+\cdots(NH_3)_n$ reactant complex was measured to be less than 10% dissociative along the O–H coordinate, whereas the $PhO\cdots H^+(NH_3)_n$ product complex ranged from 50% to 95% dissociative to form $H^+(NH_3)_n$. This work confirmed that the double-minima barrier process, modeled in Figure 1, is the correct description of the $PhOH^+$ proton-transfer reaction. However, the barrier height could not be estimated in either the picosecond work or the Mikami et al. work because the complex ion energy distribution was not known.

On the basis of the present photoelectron results showing that more than 10% of the reactant complex ions $PhOH^+\cdot NH_3$ contain at least 1 eV of energy and the previous mass spectrometry data indicating that less than 10% of the complex ions dissociate to NH_4^+,[3,8] we can place a lower limit of about 1 eV on the proton-transfer barrier height. The predicted upper limit, based on the surface crossing potential energy model summarized in Figure 1, is about 1.5 eV.

In summary, we have demonstrated a new design for molecular beam photoelectron spectroscopy and applied it to the study of the ion–molecule reactive complex $PhOH^+\cdot NH_3$. The main result is the measure of energy distributions in the ion complexes. These measurements, combined with earlier mass spectrometry measurements of proton-transfer efficiency, enable us to considerably narrow the limits on the barrier height. Future work will attempt to achieve greater cluster size specificity through the S_1 resonant intermediate step and by controlling expansion conditions. Time-resolved photoelectron measurements are also in progress.

Acknowledgment. This work was supported by the Aerospace Sponsored Research program.

References and Notes

(1) Wittig, C.; Sharpe, S.; Beaudet, R. A. *Acc. Chem. Res.* **1988**, *21*, 341. Radhakrishnan, G.; Buelow, S.; Wittig, C. *J. Chem. Phys.* **1986**, *84*, 727.
(2) Halberstadt, N.; Soep, B. *J. Chem. Phys.* **1984**, *80*, 2340.
(3) Mikami, N.; Okabe, A.; Suzuki, I. *J. Phys. Chem.* **1988**, *92*, 1858.
(4) Li, S.; Bernstein, E. R. *J. Chem. Phys.* **1992**, *97*, 792, 804.
(5) Brutschy, D.; Janes, D.; Eggert, J. *Ber. Bunsen-Ges. Phys. Chem.* **1988**, *92*, 74.
(6) Breen, J. J.; Tzeng, W.-B.; Kilgore, K.; Keesee, R. G.; Castleman, Jr., A. W. *J. Chem. Phys.* **1989**, *90*, 19.
(7) (a) Syage, J. A. *J. Chem. Phys.* **1990**, *92*, 1804. (b) Syage, J. A. *J. Phys. Chem.* **1989**, *93*, 107.
(8) Steadman, J.; Syage, J. A. *J. Am. Chem. Soc.* **1991**, *113*, 6786.
(9) (a) Syage, J. A.; Steadman, J. *J. Chem. Phys.* **1991**, *95*, 2497. (b) Steadman, J.; Syage, J. A. *J. Chem. Phys.* **1990**, *92*, 4630.
(10) Steadman, J.; Syage, J. A. *J. Phys. Chem.* **1991**, *95*, 10326.
(11) (a) Syage, J. A.; Steadman, J. *Chem. Phys. Lett.* **1990**, *166*, 159. (b) Steadman, J.; Fournier, E. W.; Syage, J. A. *Appl. Opt.* **1990**, *29*, 4962.
(12) (a) Moylan, C. R.; Brauman, J. I. *Annu. Rev. Phys. Chem.* **1983**, *34*, 187. (b) Comita, P. B.; Brauman, J. I. *Science* **1985**, *227*, 863. (c) *Gas Phase Ion Chemistry*; Bowers, M. T., Ed.; Academic Press: New York, 1979; Vols. I and II.
(13) (a) Farneth, W. E.; Brauman, J. I. *J. Am. Chem. Soc.* **1976**, *98*, 7891. (b) Jasinski, J. M.; Brauman, J. I. *J. Am. Chem. Soc.* **1980**, *102*, 2906.
(14) Steadman, J.; Syage, J. A. *Rev. Sci. Instrum.* To be published.
(15) (a) Trevor, D. J.; Van Woerkom, L. D.; Freeman, R. R. *Rev. Sci. Instrum.* **1989**, *60*, 1051. (b) Liu, G.; Barton, J. J.; Bahr, C. C.; Shirley, D. A. *Nucl. Instrum. Methods* **1986**, *A246*, 504.
(16) (a) Jouvet, C.; Lardeux-Dedonder, C.; Richard-Viard, M.; Solgadi, D.; Tramer, A. *J. Phys. Chem.* **1990**, *94*, 5041. (b) Solgadi, D.; Jouvet, C.; Tramer, A. *J. Phys. Chem.* **1988**, *92*, 3313.
(17) Lias, S. G.; Bartmess, J. E.; Liebman, J. F.; Holmes, J. L.; Levin, R. D.; Mallard, W. G. *J. Phys. Chem. Ref. Data* **1988**, *17*, 1.
(18) Lias, S. G.; Liebman, J. F.; Levin, R. D. *J. Phys. Chem. Ref. Data* **1984**, *13*, 695.